Heliyon 10 (2024) e35940

Contents lists available at ScienceDirect

Heliyon

journal homepage: www.cell.com/heliyon

Research article

Deciphering the predictive value of senescence-related signature in lung adenocarcinoma: Implications for antitumor immunity and immunotherapy efficacy

Yufeng Guo [a,b,c], Yang Wang [d], Jianchun Duan [b,c], Rui Wan [b,c], Geyun Chang [e], Xue Zhang [b,c], Zixiao Ma [b,c], Hua Bai [b,c,**], Jie Wang [b,c,*]

[a] *Department of Clinical Research, State Key Laboratory of Oncology in South China, Guangdong Key Laboratory of Nasopharyngeal Carcinoma Diagnosis and Therapy, Sun Yat-sen University Cancer Center, Guangdong Provincial Clinical Research Center for Cancer, Guangzhou, 510060, China*

[b] *National Cancer Center/National Clinical Research Center for Cancer/Cancer Hospital, Chinese Academy of Medical Sciences and Peking Union Medical College, Beijing, 100021, China*

[c] *CAMS Key Laboratory of Translational Research on Lung Cancer, State Key Laboratory of Molecular Oncology, Department of Medical Oncology, National Cancer Center/National Clinical Research Center for Cancer/Cancer Hospital, Chinese Academy of Medical Sciences and Peking Union Medical College, Beijing, 100021, China*

[d] *Department of Medical Oncology, National Cancer Center/National Clinical Research Center for Cancer/Cancer Hospital, Chinese Academy of Medical Sciences and Peking Union Medical College, Beijing, 100021, China*

[e] *Department of Thoracic Surgery, Peking University People's Hospital, Beijing, 100044, China*

ARTICLE INFO

Keywords:
Cellular senescence
FOXM1
Neutrophils
Immunotherapy
LUAD

ABSTRACT

Objective: The senescence process is pivotal in both the onset and advancement of lung adenocarcinoma (LUAD), influencing cell growth, immune evasion, the potential for metastasis, and resistance to treatments. Senescent cells' dual nature, both harmful and advantageous, adds complexity to understanding their expression patterns and clinical relevance in LUAD. In this study, we sought to evaluate the predictive value of the senescence-related signature in survival outcomes and immunotherapy efficacy in patients with LUAD.

Materials and methods: We integrated data from 1449 LUAD cases sourced from different publicly accessible datasets and a clinical cohort of Chinese LUAD patients. The Cox regression analysis employing the least absolute shrinkage and selection operator (LASSO) was performed on 156 senescence-associated genes to develop the senescence-related signature. Kaplan-Meier analysis and time-dependent receiver operating characteristic curves were utilizaed to assess the prognostic significance of the senescence-related signature. Functional annotation, immune infiltration analysis, and gene set variation analysis were applied to investigate the association of the senescence-related signature with anti-tumor immunity in LUAD. Immunotherapy cohorts of non-small cell lung cancer, urothelial carcinoma, skin cutaneous melanoma, and glioblastoma patients were included to assess the senescence-related signature in predicting immunotherapy efficacy.

* Corresponding author. National Cancer Center/National Clinical Research Center for Cancer/Cancer Hospital, Chinese Academy of Medical Sciences and Peking Union Medical College, Beijing, 100021, China.

** Corresponding author. National Cancer Center/National Clinical Research Center for Cancer/Cancer Hospital, Chinese Academy of Medical Sciences and Peking Union Medical College, Beijing, 100021, China.

E-mail addresses: baihuahb@sina.com (H. Bai), zlhuxi@163.com (J. Wang).

https://doi.org/10.1016/j.heliyon.2024.e35940
Received 12 February 2024; Received in revised form 4 August 2024; Accepted 6 August 2024
Available online 8 August 2024
2405-8440/© 2024 Published by Elsevier Ltd. This is an open access article under the CC BY-NC-ND license (http://creativecommons.org/licenses/by-nc-nd/4.0/).

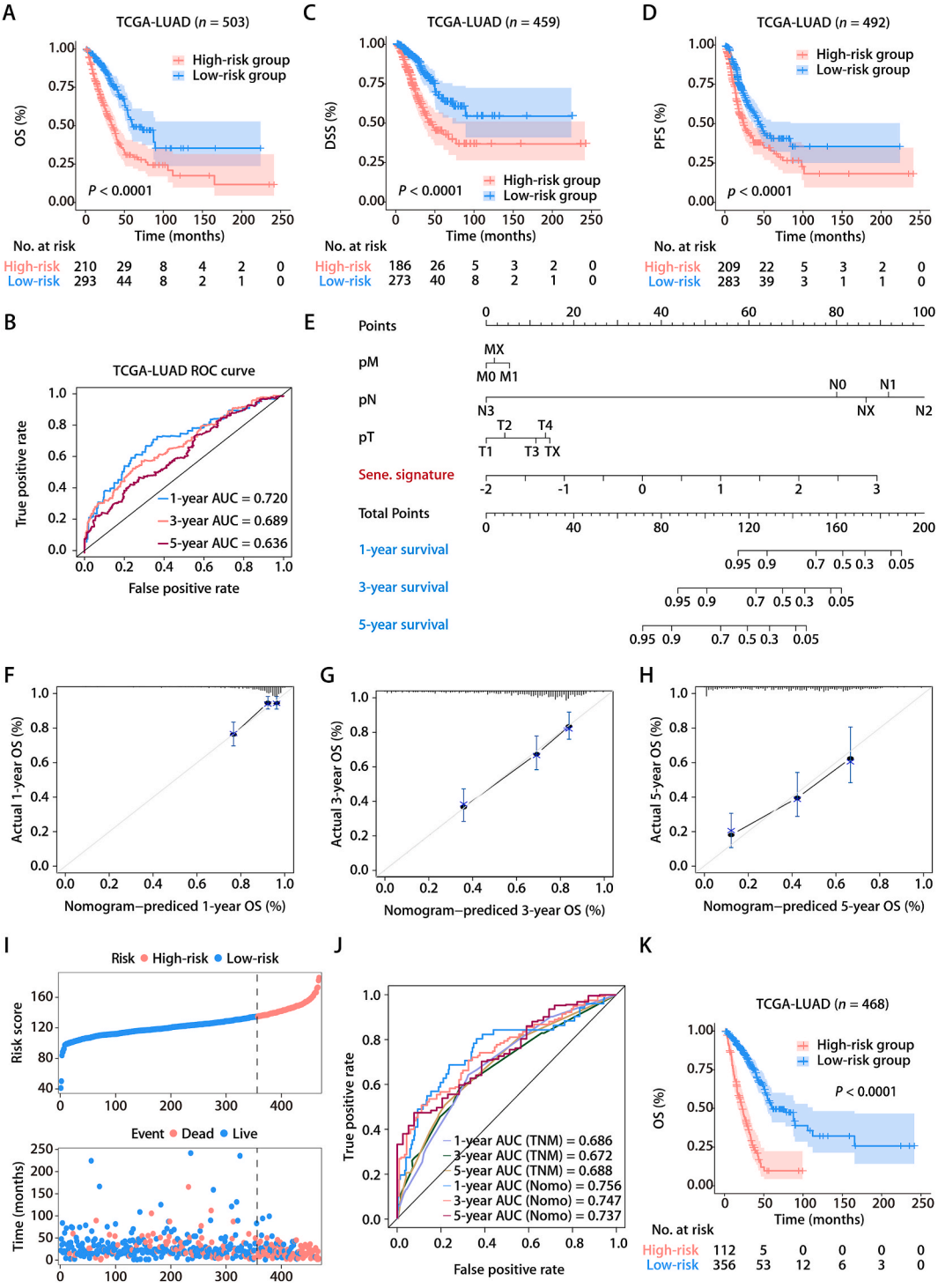

Fig. 1. Identification and establishment of the senescence-related signature.
(A–C) K-M survival analysis of OS (A), DSS (B), PFS (C) between the high-risk and low-risk groups stratified by the senescence-related signature in the TCGA-LUAD cohort. (D) AUC values of ROC predicted 1-, 3- and 5-year OS of the signature in the TCGA-LUAD cohort.(E) The nomogram for predicting the 1-, 3-, and 5-year OS of patients in the TCGA-LUAD cohort.(F–H) The calibration curve for predicting patients' OS at 1- (F), 3- (G), and 5-year (H).(I) The distributions of the risk score calculated by the nomogram and survival status of TCGA-LUAD patients.(J) Time-dependent ROC analysis to assess the predictive function of the nomogram and TNM staging system at 1, 3, and 5 years.(K) K-M survival analysis of OS between the high- and low-risk patients stratified by the senescence-related nomogram in the TCGA-LUAD cohort.

Results: The senescence-related signature, which encompasses seven senescence-related genes, namely, *FOXM1*, *VDAC1*, *PPP3CA*, *MAPK13*, *PIK3CD*, *RRAS*, and *CCND3*, was identified to have predictive significance across multiple LUAD cohorts and demonstrated a negative association with antitumor immunity and tumor-infiltrating neutrophils. Patients exhibiting low expression levels of the senescence-related signature responded more favorably to immune checkpoint inhibitors in various solid tumors, including LUAD. Inhibiting FOXM1 pharmacologically with thiostrepton produced tumor-suppressive effects and improved immunotherapy responses in a Lewis lung carcinoma mouse model.
Conclusions: The senescence-related signature demonstrates potential in predicting patient prognosis and immunotherapy efficacy in LUAD.

1. Background

Lung adenocarcinoma (LUAD), the most common form of non-small cell lung cancer (NSCLC), is one of the most frequently identified cancers around the globe [1]. Immune checkpoint inhibitors (ICIs) targeting programmed cell death-1 (PD-1) and its ligand PD-L1 have transformed the treatment paradigm and shown response rates of up to 40 % in late-staged LUAD patients [2]. However, only a small proportion achieves durable remission with ICIs [3]. Thus, it is essential to discover new biomarkers of patient prognosis and immunotherapy outcome and understand the mechanisms underlying the responsiveness to ICIs in LUAD.

Cellular senescence entails a stable status of cell cycle arrest in which cells cease to divide despite growth factors and mitogenic signals [4]. DNA damage, telomere dysfunction, oncogene activation, and organelle stress can trigger cellular senescence, which plays a role in tumor suppression, tissue repair, embryonic development, and aging [4]. Research indicates that senescence prevents precancerous cells proliferation and facilitates their elimination through immune surveillance [5]. However, insufficient immune surveillance and the subsequent failure to eliminate senescent cells may lead to chronic inflammation and a pro-tumorigenic niche that supports cancer initiation, progression, and metastasis [5]. While some studies highlight senescent cells' role in enhancing immune-mediated clearance, others point to senescence-driven immune responses as immunosuppressive and tumor-promoting [6]. Prolonged inflammatory conditions within the tumor microenvironment (TME) have the potential to facilitate an immunosuppressive state, a phenomenon that may also apply to a senescent environment [7]. Yet, the landscape of cellular senescence in antitumor immunity and the immunotherapy response of LUAD remains underexplored, indicating a necessity for further research into how cellular senescence empowers the remodeling of the immunosuppressive TME and the development of novel senescence-based immunotherapeutic approaches.

Our study focused on the expression and clinical relevance of senescence-associated genes, leading to the establishment of a predictive signature, the senescence-related signature, for LUAD. This signature, closely linked with patient outcomes, outperformed conventional staging systems in predicting survival in seven independent validation cohorts. We also developed a comprehensive nomogram to estimate the overall survival (OS) probability in LUAD patients. Functional analyses suggested that the senescence-associated signature may contribute to an unfavorable prognosis by suppressing the systemic neutrophil response in patients with LUAD.

2. Results

2.1. Establishment of the senescence-related signature

One hundred fifty-six senescence-related genes were initially selected from the Molecular Signatures Database (MSigDB). Then, we identified senescence-related genes with prognostic significance via the least absolute shrinkage and selection operator (LASSO) method (Figs. S1A and S1B). The Cox regression analysis further narrowed down the selection to seven genes with the highest predictive value for LUAD prognosis: *FOXM1*, *VDAC1*, *PPP3CA*, *MAPK13*, *PIK3CD*, *RRAS*, and *CCND3* (Fig. S1C). The risk score was calculated using a formula that integrates gene expression levels weighted by their respective coefficients from the Cox model: risk score = (0.15456 × *FOXM1*) + (0.17907 × *VDAC1*) + (−0.38644 × *PPP3CA*) + (−0.16558 × *MAPK13*) + (0.18365 × *PIK3CD*) + (0.27251 × *RRAS*) + (0.27251 × *CCND3*). A close relationship was revealed between the expression patterns of the seven senescence-related genes and the risk score, as shown in Fig. S1C. The group at high risk experienced markedly poorer survival outcomes than did the low-risk group according to Kaplan-Meier (K-M) analysis of OS (Fig. 1A). Time-dependent receiver operating characteristic (ROC) curves were also used to test the prognostic significance. The area under the curve (AUC) for 1-year, 3-year, and 5-year OS were 0.720, 0.689, and 0.636, respectively. (Fig. 1B). Moreover, the senescence-related signature showed significant prognostic value when applied to disease-specific survival (DSS; Fig. 1C) and progression-free survival (PFS; Fig. 1D). The necessity to stratify patients by early and advanced stages due to differing therapeutic needs and prognostic outlooks led us to apply the signature within these specific subsets. The analyses confirmed that the signature retained its prognostic significance for OS regardless of tumor stages (Figs. S2A and S2B) of LUAD. We extended our analysis to scrutinize the senescence-related signature's performance across varying clinicopathological features and mutation profiles, such as *EGFR* and *KRAS*. K-M analyses consistently demonstrated that high-risk scores predicted shorter OS across all subgroups (Figs. S2C–S2H). Similarly, the risk groups based on our signature provided a significant stratification of OS in different genetic mutation contexts (Fig. S3). The senescence-related signature was also identified to be a significant predictor

of OS based on univariate and multivariate statistical approaches (Tables S1 and S2).

With the independence of the signature established, we formulated a predictive nomogram integrating the senescence-related signature with the TNM staging system in TCGA-LUAD cohort (Fig. 1E). The nomogram's predictive accuracy was validated using calibration curves (Fig. 1F–H). The distribution of patient survival and calculated risk scores based on the nomogram are shown in Fig. 1I. The AUC for 1-, 3-, and 5-year OS were 0.756, 0.747, and 0.737, respectively (Fig. 1J), which outperformed the TNM staging system in predicting patient prognosis (Fig. 1J). Patients classified as low-risk by the senescence-related signature-based nomogram had survival advantage than did those in the high-risk group (Fig. 1K). The senescence-related signature was found to be a significant prognostic factor in multiple cancer types, including LUAD (Fig. S4). These data reinforced the robustness of the senescence-related signature across various solid tumors, supporting its translational potential in prognostic prediction.

2.2. Validation of the senescence-related signature

By calculating risk values for patients in six independent GEO datasets, we confirmed statistically significant differences in survival probabilities of the risk-defined groups in the GSE50081 (Fig. 2A), GSE26939 (Fig. S5A), and GSE32019 (Fig. 2B) cohorts. The AUC for 1-, 3-, and 5-year OS were 0.708, 0.674, and 0.610, respectively, in the GSE50081 cohort (Fig. 2C). Similar results were obtained in the GSE26939 (Fig. S5B) and GSE32019 cohorts (Fig. 2D). Significant differences were detected in the disease-specific survival (DSS) in the GSE50081 cohort (Fig. 2E). The AUC values predicting 1-, 3-, and 5-year DSS were 0.658, 0.645, and 0.624, respectively (Fig. 2F). Analyses based on the GSE13123 (Fig. S5C), GSE72094 (Fig. S5D), and GSE29016 (Fig. S5E) cohorts also suggested predictive

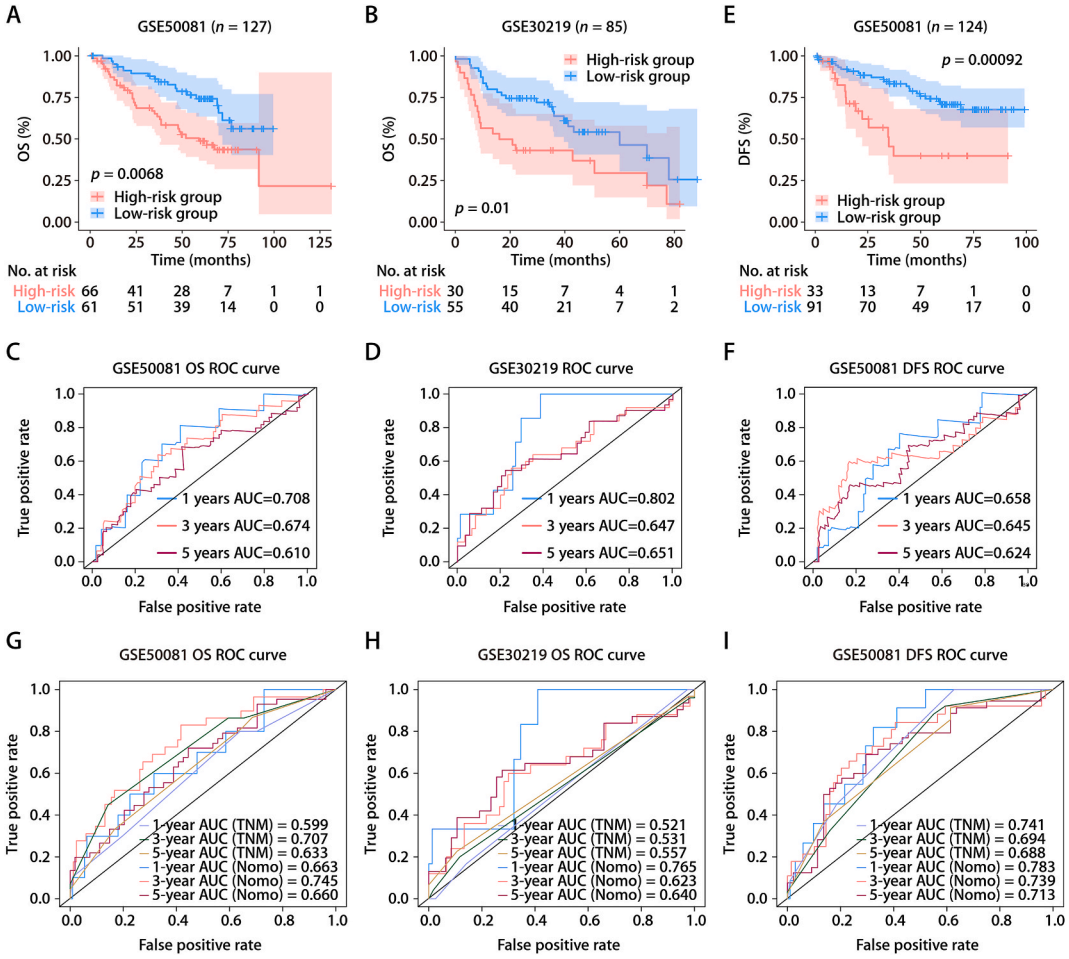

Fig. 2. Validation of the senescence-related signature in GEO LUAD cohorts
(A and B) K-M curves of OS between the high- and low-risk groups of LUAD patients (lower panel) in the GSE50081 (A) and GSE30219 (B) datasets. (C and D) AUC values of ROC predicted 1-, 3- and 5-year OS of the signature in the GSE50081 (C) and GSE30219 (D) datasets. (E) K-M curve of DFS between the high- and low-risk groups of LUAD patients in the GSE50081 dataset. (F) AUC values of ROC predicted 1-, 3- and 5-year DFS of the signature in the GSE50081 dataset. (G and H) Time-dependent ROC analyses to assess the predictive function of the nomogram and TNM staging system at 1-, 3-, and 5-year OS of patients in the GSE50081 (G) and GSE30219 (H) datasets. (I) Time-dependent ROC analysis to assess the predictive function of the nomogram and TNM staging system at 1-, 3-, and 5-year DFS of patients in the GSE50081 datasets.

potential for LUAD patient outcomes. Consistent with the TCGA-LUAD cohort results, the prognostic significance was confirmed across multiple LUAD cohorts (Tables S1 and S2). Furthermore, we validated the senescence-based nomogram across various LUAD cohorts. We confirmed the nomogram's performance for estimating the OS (Figs. S6 and S7) and DFS (Fig. S8) probabilities in LUAD patients. Similarly, we observed the nomogram's better performance in predicting patient prognosis than that of the TNM staging system across various LUAD cohorts (Fig. 2G–I, S5F, and S5G).

2.3. Functional annotation of the senescence-related signature

Given the senescence-related signature's predictive power, our next goal was to understand the signature-associated biological function. Genes between the risk-defined groups, showing a |log2 fold change| of expression greater than 1 and a *P* value less than 0.05, were considered differentially expressed genes (DEGs). Analysis of hallmark gene sets revealed significant enrichment (adjusted *P*

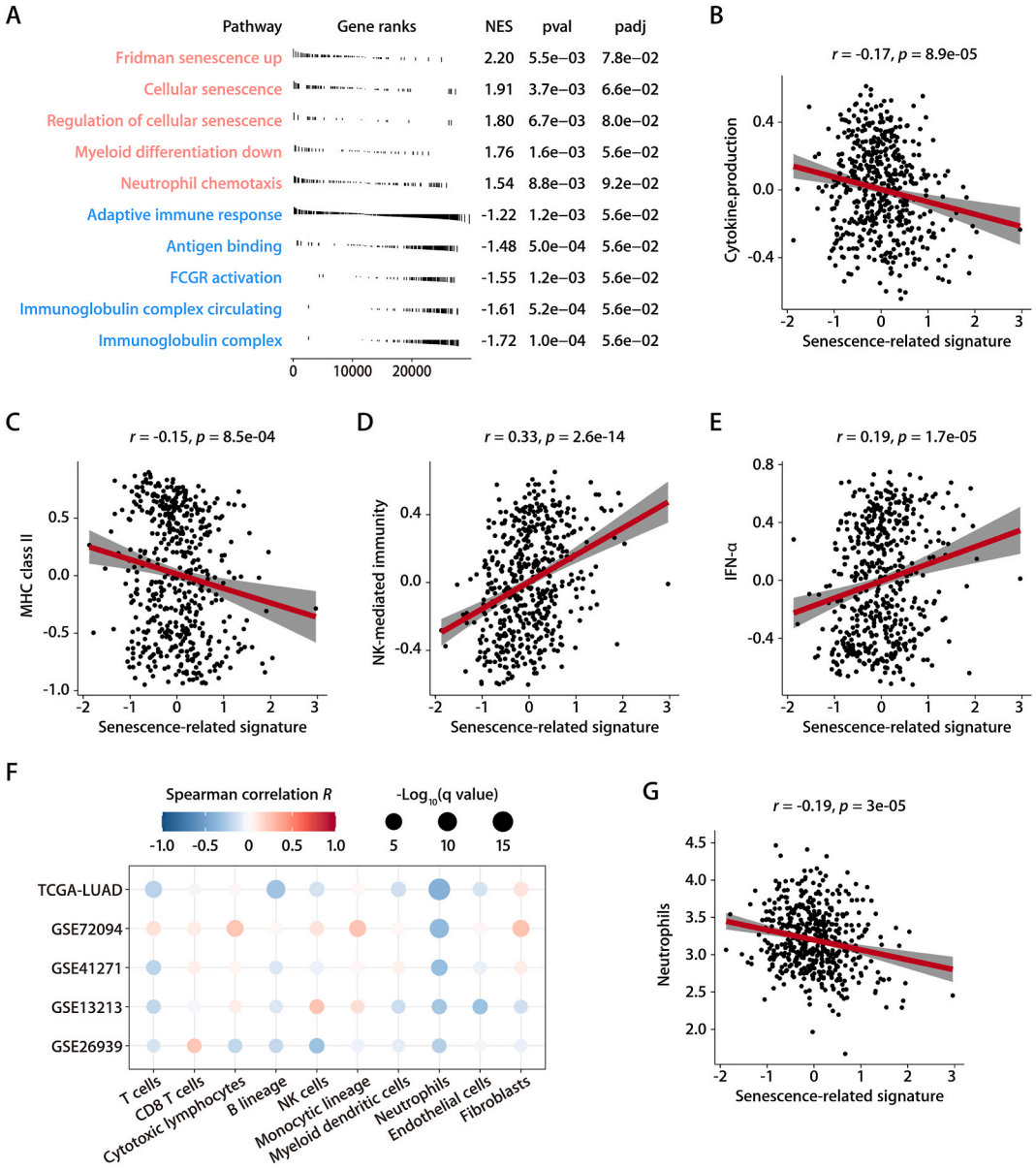

Fig. 3. Relationship between the senescence-related signature and anti-tumor immunity in LUAD
(A) Significantly enriched gene sets based on the DEGs between the high- and low-risk groups in the TCGA-LUAD. (B–E) The correlation analysis between risk score and immune metagenes involved in cytokine production (B), MHC class II (C), NK-mediated immunity (D), and IFN-α signaling (E). (F) Heatmap depicting the correlation between risk score and the infiltration of immune cells inferred by MCP-counter across various LUAD cohorts. (G) The correlation analysis between risk score and neutrophils.

value < 0.01) of the downregulated genes in adaptive immunity and antigen binding. In contrast, the upregulated genes were mainly associated with cellular senescence, myeloid differentiation, and neutrophil chemotaxis (Fig. 3A). Immune metagene analysis of the senescence-related signature suggested negative correlations with cytokine production and MHC-II complex expression and positive correlations with NK-mediated immunity and IFN-α signaling (Fig. 3B–E). Recent evidence reported that senescent cells, particularly when they persist, activated a robust type I interferon response [8], which has been partially attributed to the reactivation of transposable elements and the cyclic GMP–AMP synthase (cGAS)-stimulator of interferon genes (STING) pathway [8,9]. These findings suggest that senescent cells may remodel the immunosuppressive TME, in part, through IFN-α signaling pathways.

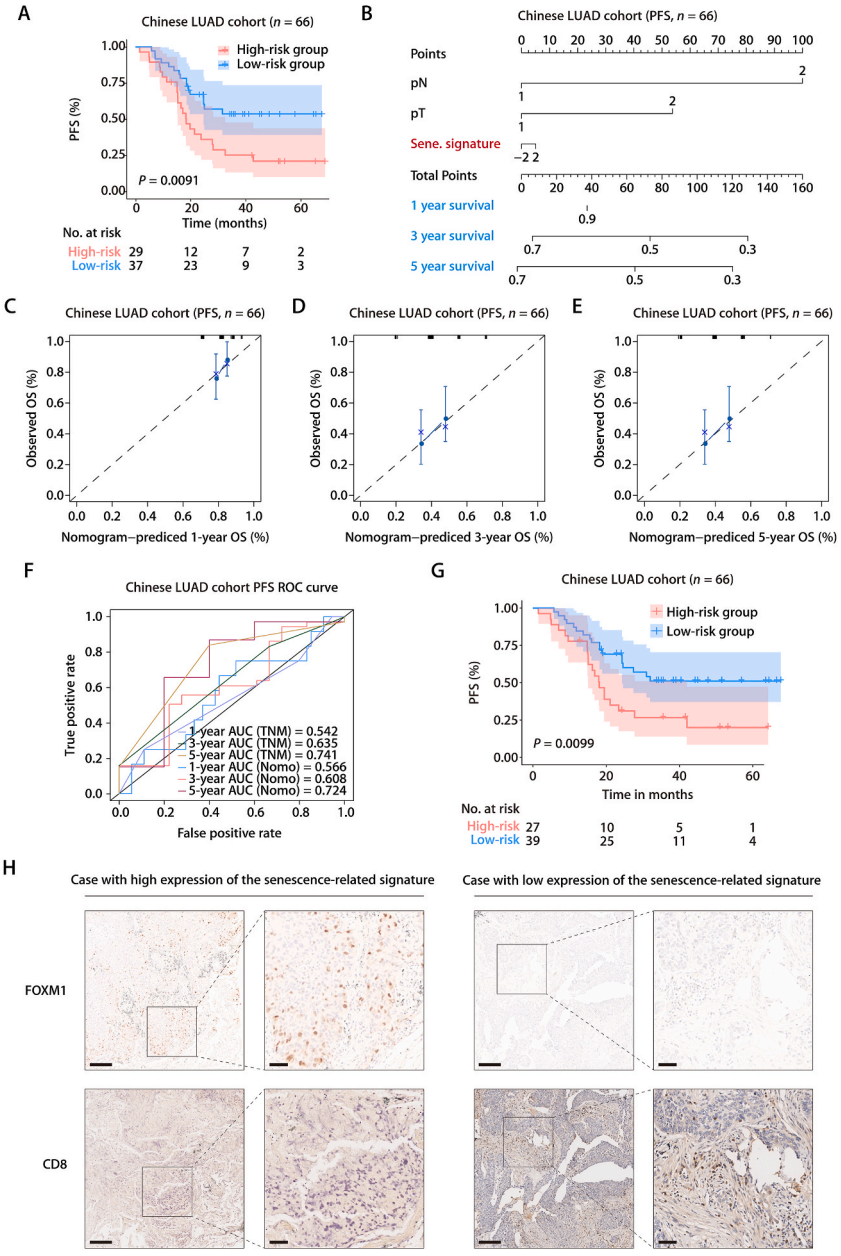

Fig. 4. Evaluation of the senescence-related signature in the Chinese LUAD cohort.
(A) K-M survival analysis of DFS between the high- and low-risk groups in the Chinese LUAD cohort. (B) The nomogram for predicting the 1-, 3-, and 5-year OS of patients in the Chinese LUAD cohort.(C–E) The calibration curve for predicting patients' PFS at 1- (C), 3- (D), and 5-year (E).(F) Time-dependent ROC analysis to assess the predictive function of the nomogram and TNM staging system at 1-, 3-, and 5-year PFS of patients in the Chinese LUAD cohort.(G) K-M survival analysis of PFS between the high- and low-risk patients stratified by the senescence-related nomogram in the Chinese LUAD cohort. (H) Representative microscopic images of FOXM1 expression and $CD8^+$ T cells in tissue samples patients in the Chinese LUAD cohort. The scale bars represent 200 μm (left panel) and 50 μm (right panel) in each case, respectively.

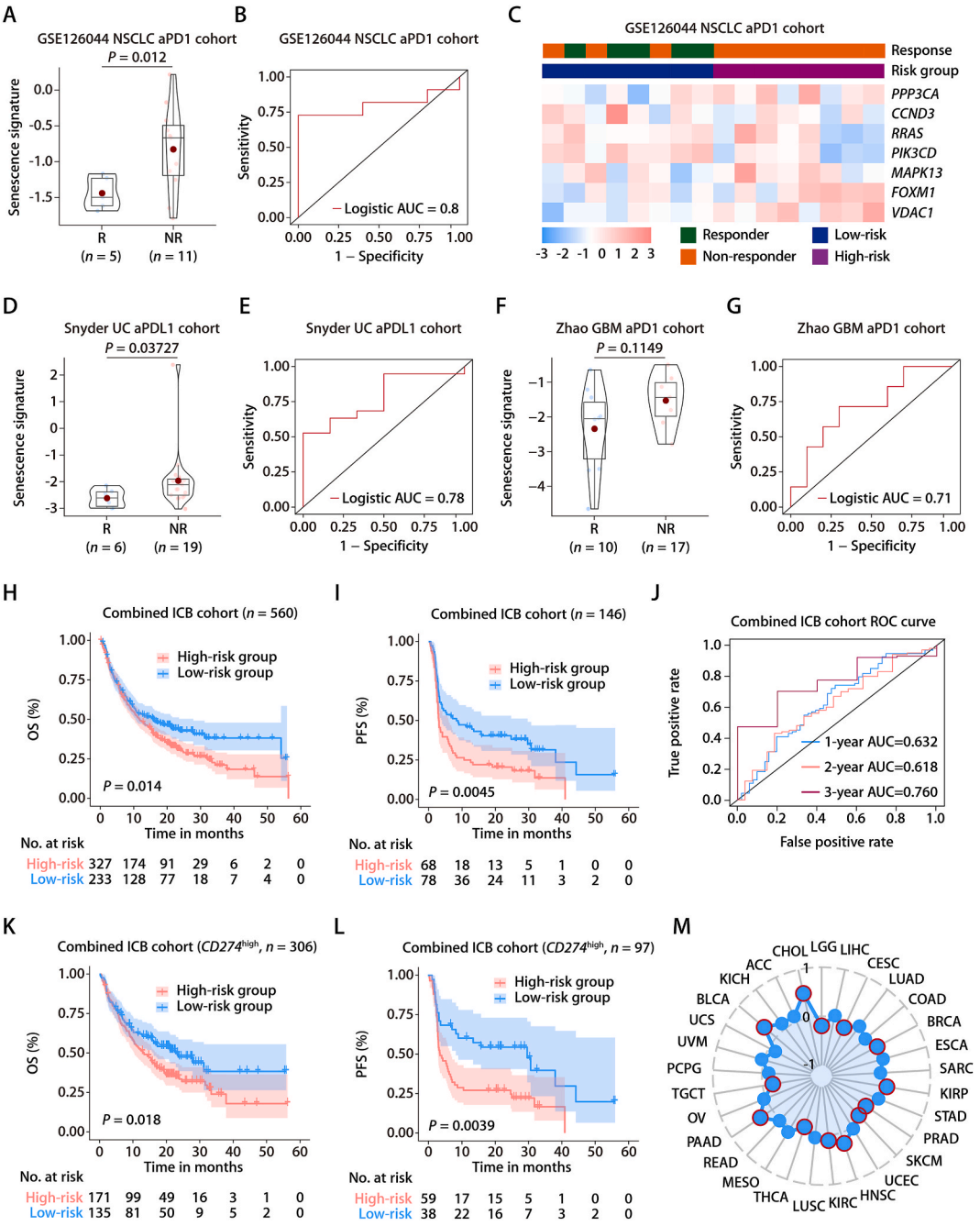

Fig. 5. The predictive value of the senescence-related signature on immunotherapy efficacy.
(A) The distributions of the risk scores between responders and non-responders to anti-PD-1 therapy in the GSE126044 NSCLC anti-PD-1 cohort. (B) Logistic ROC analysis of the senescence-related signature in stratifying responders and non-responders in the GSE126044 NSCLC anti-PD-1 cohort. (C) The expression pattern of the senescence-related gene signature and response to anti-PD-1 therapy in the GSE126044 NSCLC anti-PD-1 cohort. (D) The distributions of the risk scores between responders and non-responders in the Snyder UC anti-PD-L1 cohort. (E) Logistic ROC analysis of the senescence-related signature in stratifying responders and non-responders in the Snyder UC anti-PD-L1 cohort. (F) The distributions of the risk scores between responders and non-responders in the Zhao GBM anti-PD-1 cohort. (G) Logistic ROC analysis of the senescence-related signature in stratifying responders and non-responders in the Zhao GBM anti-PD-1 cohort. (H and I) K-M survival analysis of OS (H) and PFS (I) between the high- and low-risk groups in the combined immunotherapy cohorts. (J) AUC values of ROC predicted 1-, 2- and 3-year PFS of the signature in the combined immunotherapy cohorts. (K and L) K-M survival analysis of OS (F) and PFS (L) between the high- and low-risk groups of patients with high *CD274* mRNA expression in the combined immunotherapy cohorts. (M) Circos plot depicting the Pearson correlation between the senescence-related signature and *CD274* mRNA expression in TCGA pan-cancer cohorts. The red circle indicates a significant correlation.

Tumors with high-risk scores exhibited dampened T cells, NK cells, and macrophage infiltration in TCGA-LUAD cohort (Fig. S9A). Notably, statistically significant negative correlations between the senescence-related signature and neutrophils were observed across training and validation cohorts (Fig. 3F). In comparison with the high-risk group, significantly higher infiltration of neutrophils (Fig. 3G) and T cells (Fig. S9B) was observed in the low-risk group. This is particularly relevant as higher neutrophil infiltration has been recently linked to better responses to immunotherapy [10].

We thoroughly analyzed the senescence-related signature and 43 immune-related genes [11] and showed a primarily negative relationship across training and validation cohorts (Fig. S9C). Specifically, the signature exhibited negative and positive associations with the co-stimulatory gene *CD28* and inhibitory genes like *CD276*, *VTCN1*, and *EDNRB*, respectively (Fig. S9C). These results indicate that tumors with low expression of the senescence-related signature demonstrate stronger antitumor immunity.

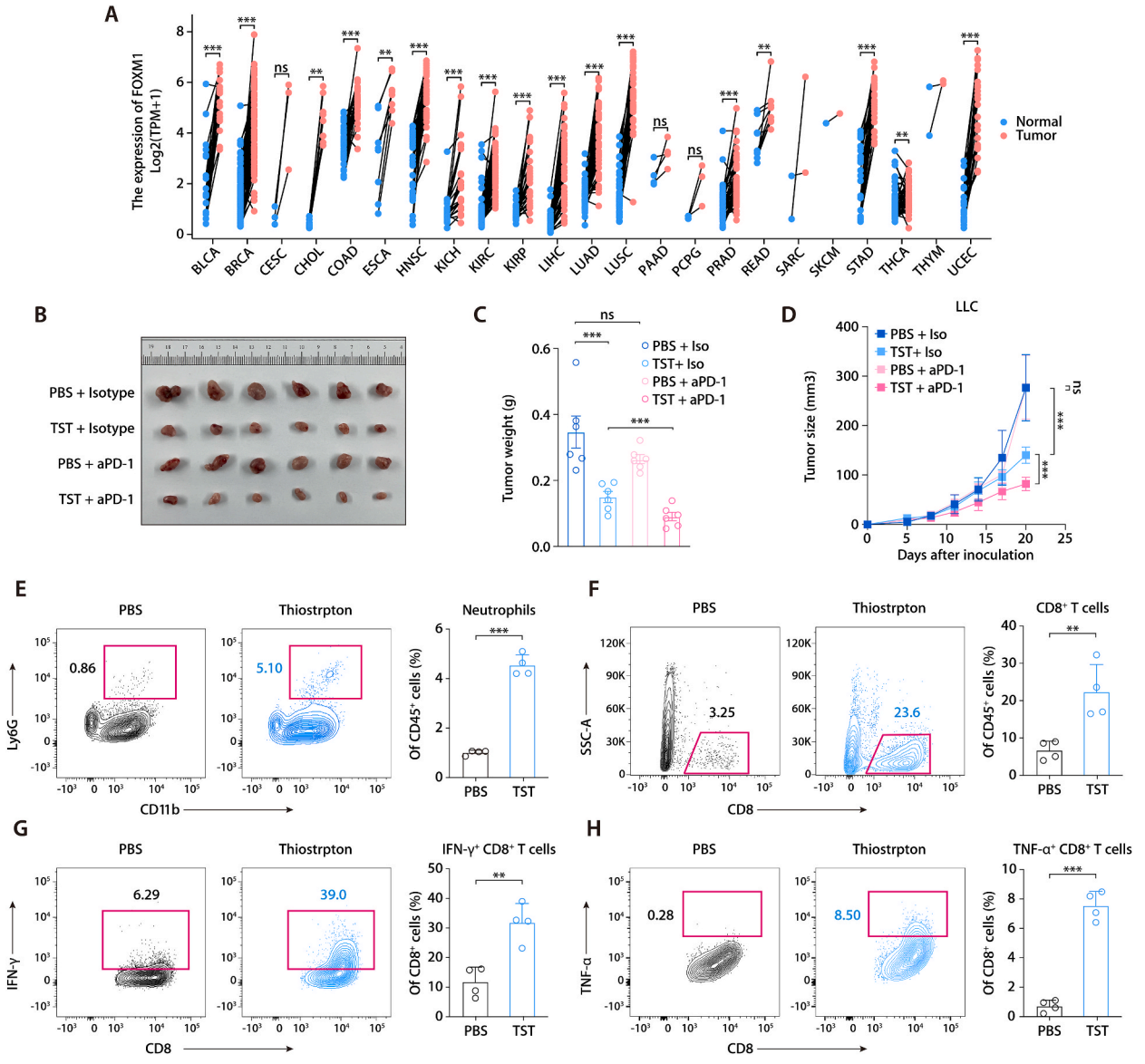

Fig. 6. The translational potential of FOXM1 inhibition

(A) Comparison of *FOXM1* mRNA expression between tumor tissue and normal counterparts of TCGA pan-cancer dataset. (B) The representative image of LLC tumors receiving PBS plus Isotype, TST plus isotype, PBS plus anti-PD-1, and TST plus anti-PD-1. (C) LLC tumor weights of different treatment groups ($n = 6$/group) as described in (A). (D) LLC tumor volumes of different treatment groups ($n = 6$/group) as described in (A). (E–H) Mice ($n = 4$/group) were treated as described. Single-cell suspension was prepared from tumors at day 10 and analyzed by flow cytometry. Representative flow plots are shown for events gated on live $CD45^+CD11b^+Ly6G^+$ (tumor-infiltrating neutrophils, E), $CD45^+CD8^+$ ($CD8^+$ T cells, F), $CD45^+CD8^+IFN\text{-}\gamma^+$ (G), and $CD45^+CD8^+TNF\text{-}\alpha^+$ (H). Percentage of neutrophils/$CD45^+$ cells ± SEM, neutrophils/$CD45^+$ cells ± SEM, $CD45^+CD8^+IFN\text{-}\gamma^+/CD8^+$ T cells ± SEM, and $CD45^+CD8^+TNF\text{-}\alpha^+/CD8^+$ T cells ± SEM are quantified per treatment. Each symbol represents a mouse.

2.4. The senescence-related signature in the Chinese LUAD cohort

We next conducted further validation in an independent Chinese LUAD cohort comprising 66 tissue samples with panel transcriptomic sequencing (Fig. S10A). A notable difference in PFS was observed between the risk-defined groups (Fig. 4A). Cox regression analysis identified a significantly elevated risk impacting patient outcomes in this cohort (Tables S1 and S2). The senescence-related signature remained a significant factor in determining PFS in the Chinese LUAD cohort (Fig. S10B), further validating its robustness in predicting LUAD patient survival. Additionally, the senescence-based nomogram (Fig. 4B) demonstrated high accuracy, calibration (Fig. 4C–E), and discrimination potential (Fig. 4F and G) for estimating PFS probability. Similar to the functional annotation results, immunohistochemistry (IHC) analysis of tumor tissue from this cohort revealed that FOXM1 expression was negatively correlated with CD8 protein expression (Fig. 4H).

2.5. Predictive value of the senescence-related signature on immunotherapy efficacy

We next conducted analysis of the GSE126044 NSCLC anti-PD-1 cohort to evaluate the senescence-related signature in predicting immunotherapy efficacy. The risk scores showed statistically significant differences between responders and non-responders (Fig. 5A). The robustness in determining the responsiveness was highlighted by an AUC of 0.8 (Fig. 5B). The expression of senescence-related genes were associated with immunotherapy efficacy, with *FOXM1*, *VDAC1*, and *PPP3CA* negatively correlated, and *CCND3*, *RRAS*, and *PIK3CD* positively correlated with objective response status (Fig. 5C). The signature was significantly associated with immunotherapy efficacy (Fig. 5D–G), achieving AUC values of 0.78 and 0.71, in urothelial carcinoma (UC) and glioblastoma (GBM) patients treated with ICIs, respectively (Fig. 5E and G). Although the difference in the risk scores between responders and non-responders in the Zhao GBM anti-PD1 cohort was not statistically significant, there was indeed a numerical trend showing higher scores in non-responders compared to responders (Fig. 5F). Furthermore, we combined data from immunotherapy cohorts of UC, skin cutaneous melanoma (SKCM), and GBM patients. After normalizing the data, we calculated the senescence-related signature scores for each patient and observed that the high-risk group had shorter OS and PFS than did the low-risk group (Fig. 5H and I). The AUC for 1-, 2-, and 3-year PFS were 0.632, 0.618, and 0.760, respectively (Fig. 5J). Specifically, the high-risk group exhibited shorter OS in the Mariathasan UC anti-PDL1 cohort (Fig. S11A). A similar result was observed for PFS in the Liu SKCM anti-PD1 cohort (Figs. S11B and S11C). Compared to IMS.Sig [12], IMPRES.Sig [13], LRRC15.CAF.Sig [14], CRMA.Sig [15], IPRES.Sig [16], and TcellExc.Sig [17], the senescence-related signature showed favorable performance in NSCLC, UC, GBM, and SKCM immunotherapy cohorts (Figs. S11D and S11E).

Since PD-L1 expression is currently the standard test for determining tumor susceptibility to checkpoint inhibitors, we next evaluated the correlation of the signature and PD-L1 expression. A high-risk score was associated with shorter OS (Fig. 5K) and PFS (Fig. 5L) in patients with relatively higher *CD274* mRNA expression (which encodes PD-L1). Although the survival differences (OS and PFS) did not reach statistical significance in patients with relatively lower *CD274* mRNA expression (Figs. S11F and S11G), likely due to sample size, a numerical trend for longer OS and PFS was seen in the low-risk group as compared to the high-risk group. Importantly, the signature did not correlate significantly with *CD274* mRNA expression (Figs. S12A and S12B). Besides, no significant correlation between the signature and PD-L1 expression was found in various solid tumors (Fig. 5M) and immunotherapy cohorts (Figs. S12C–S12F), indicating that the potential of the signature in predicting immunotherapy outcome is not dependent on PD-L1 expression.

2.6. The translational potential of pharmacological inhibition of FOXM1

FOXM1 exhibited upregulated expression compared to normal tissue counterparts in several solid tumors, including LUAD and LUSC (Fig. 6A). TST is recognized as an inhibitor of protein synthesis and has been documented to suppress FOXM1, influencing the aggressive characteristics of diverse tumors such as those found in colorectal, breast, lung, and ovarian cancer, as well as acute lymphoblastic leukemia and pancreatic cancer [18]. However, how it affects the immunosuppressive TME and the responsiveness to immunotherapy remains unclear. Using the TST and LLC mouse models, we discovered that pharmacological inhibition of FOXM1 dampened tumor growth and enhanced immunotherapy efficacy (Fig. 6B–D). Specifically, TST treatment triggered the neutrophil response and promoted $CD8^+$ T cell infiltration and cytotoxicity (Fig. 6E–H).

3. Discussion

Cellular senescence plays pro-tumor and anti-tumor roles depending on the specific spatial and temporal context [19]. It is crucial to recognize that elements of the senescence-associated secretory phenotype (SASP), primarily consisting of pro-inflammatory cytokines such as interleukin-6 (IL-6) and IL-8, can attract various immune cells, such as NK cells, T cells, and macrophages [20–22]. The immunological recognition and elimination of senescent cells are essential for preventing tumorigenesis, particularly in premalignant states and following cancer treatment [23]. On one hand, senescent cancer cells recruit T cells that in turn trigger senescence in tumor cells to inhibit tumor progression. This underscores the critical role of cellular senescence in immune surveillance [24,25]. On the other hand, cellular senescence can promote cancer development through impaired immune surveillance and the induction of immunosuppressive responses [26,27]. Inducing senescence in tumor cells has been observed to induce pro-tumor $Gr\text{-}1^+$ myeloid cell infiltration, thereby contributing to ongoing tumor development and resistance to chemotherapy [28,29].

As inflammatory cells, neutrophils can secrete various cytokines that affect cancer cell survival [30]. Interactions between

neutrophils and other immune cells remodels an immunosuppressive environment that supports primary tumor growth [31]. However, recent studies suggest anti-tumor properties of neutrophils. For example, neutrophil-derived reactive oxygen species (ROS) can activate a Ca^{2+} channel in cancer cells, leading to cell death [32,33]. Tumor-entrained neutrophils (TENs) can inhibit tumor spread by producing hydrogen peroxide (H_2O_2) [34]. Neutrophils significantly impact the tumor TME through pro- and anti-tumor interactions with various cells [31]. The precise molecular mechanisms remain unclear.

The function of voltage-dependent anion channel 1 (VDAC1) extends beyond energy metabolism to include associations with neurodegenerative and cardiovascular diseases, diabetes, and various cancers, positioning it as a primising target [35]. PPP3CA, the gene encoding calcineurin A, plays a crucial role in immunomodulation [36]. Moreover, the effect of PPP3CA knockdown on T cell proliferation and cytokine production [37] underscore its influence on tumor immunology. We also explored MAPK13, encoding p38δ [38], the lack of which has underscored its role in various inflammatory diseases and cancers [39,40]. Biochemical evidence suggests that p38γ/δ are important in myeloid cells [38], and their absence results in reduced cytokine and chemokine production [40]. PI3Kδ, frequently upregulated in both hematologic malignancies [41] and solid tumors [42,43], has become a focus as a therapeutic target [44]. R-Ras regulates apoptosis [45,46] and integrin-mediated cell adhesion, which affects cell survival and matrix assembly [47,48]. Lastly, CCND3, a cyclin whose timely degradation is crucial for cell cycle progression, has been implicated in multiple myeloma (MM) and other solid tumors [37,49]. Its dysregulation, particularly in MM cells with specific chromosomal translocations and mutations [50], has led to its consideration as a marker for a molecular subtype of MM [51,52]. In sum, these findings not only shed light on the multifaceted roles of these genes in LUAD pathology and their potential as prognostic markers but also emphasize their involvement in the intricate dynamics of tumor immunology and treatment response.

Transcriptomic profiling of LUAD has consistently demonstrated the immunosuppressive TME within tumors with high senescence-related signature expression. Tumor-infiltrating neutrophils exhibit transcriptomic and functional heterogeneity [53,54]. Hence, we analyzed the relationship between neutrophils and the senescence-related signature. Interestingly, a negative association between tumor-infiltrating neutrophils and the senescence-related signature was observed. Meanwhile, FOXM1 exhibited an upregulated expression pattern in tumor tissue compared to normal counterparts. Further experimental investigation revealed a close relationship between FOXM1 and tumor-infiltrating neutrophils and T-cell immunity. Notably, neutrophils that were activated by therapy exhibited an interferon gene signature. These interferon-responsive neutrophils, particularly dependent on the transcription factor IRF1, were crucial for the effectiveness of immunotherapy, with their absence leading to treatment failure [10]. Our study has provided insights into the role of tumor-infiltrating neutrophils in regulating TME remodeling and its responsiveness to immunotherapy. Indeed, tumors with a high expression of the senescence-related signature exhibited pronounced immunosuppressive characteristics, supporting the signature's value in prognosis prediction.

The study has certain limitations. Firstly, the tissue samples tested by IHC were from treatment-naïve patients undergoing surgery. The study requires further examination of tissue samples from LUAD patients receiving immunotherapy. This would help demonstrate its predictive value for immunotherapy outcomes. Secondly, the underlying mechanism of the senescence-related signature affecting neutrophil response warrants further exploration.

4. Conclusion

Cellular senescence is crucial in LUAD tumorigenesis and progression. The study explored senescence-associated genes' expression pattern and clinical significance. We developed a predictive model and validated its capacity across various LUAD cohorts. The findings of this study have implications for guiding patient stratification and enhancing immunotherapy efficacy for patients with LUAD.

5. Materials and methods

5.1. Risk stratification of patients based on the senescence-related signature

Risk stratification was performed via the 'survivalROC' package [55] in R.

6. Panel RNA-seq of LUAD samples

Between May 2013 and September 2018, a total of 66 frozen LUAD tissue samples from the National Cancer Center/Cancer Hospital, Chinese Academy of Medical Sciences was collected and underwent panel RNA-seq according to the manufacturer's guidelines. The relevant ethics committee approved the study protocols, and informed consent was obtained from all patients. Patient information and RNA-seq data are listed in Tables S3 and S4, respectively.

7. Animal studies

Tumor expansion was recorded three times a week. Mice were humanely euthanized when the principal dimension reached 15 mm. When tumors grew to 25–50 mm^3, mice were divided into groups receiving intraperitoneal injections of thiostrepton (TST) (100 μg per mouse) or phosphate-buffered saline (PBS) (negative control), along with anti-PD-1 (200 μg per mouse) or isotype control every three days for a total of three injections.

8. Cell culture

The syngeneic mouse LLC was purchased from the American Type Culture Collection and cultured in Dulbecco's modified Eagle's medium (DMEM) containing 10 % fetal bovine serum (FBS) and 100 U/mL penicillin/streptomycin at 37 °C in a 5 % CO_2 humidified atmosphere. Cell culture was tested and found to be mycoplasma-free.

8.1. Flow cytometry

LLC cell line grafts were harvested from mice when they reached about 500 mm^3 in volume, weighed, and subsequently finely chopped. They were then dissociated enzymatically using collagenase I at a concentration of 500 U/mL (Sigma-Aldrich, United States) alongside 200 mg/mL DNAse I (Roche, Switzerland) for 30 min at 37 °C. Post-incubation, the mixtures were filtered through a mesh of 70 μm to eliminate sizeable undigested tissue fragments. We used a specific Lysis Solution (Qiagen, Netherlands) to lyse red blood cells. In preparation for cell surface marking, we treated one million cells with an anti-Fc receptor-blocking antibody (clone 2.4G2). We selected and mixed appropriate antibodies in a buffer suited for surface staining, maintaining the cells on ice for half an hour. Cells underwent fixation and permeabilization and were then subjected to intracellular cytokine staining. The gating strategy involved selecting single, viable cells and employing a combination of markers to identify specific immune populations: tumor-infiltrating neutrophils: $CD45^+CD11b^+Ly6G^+$; $CD8^+$ cytotoxic T cells: $CD45^+CD3^+CD8^+$; IFN-γ^+CD8^+ T cells: $CD45^+CD3^+CD8^+$IFN-γ^+; TNF-α^+CD8^+ T cells: $CD45^+CD8^+$TNF-α^+.

8.2. Statistical analysis

Student-t-test was used to compare differences between the risk-defined groups. Pearson analysis was utilized to evaluate the correlation. The Wilcoxon test was employed to compare immune cell infiltration. P value less than 0.05 was considered statistically significant.

Data availability

The Results section listed the accession numbers of publicly available datasets. The Supplementary files included information concerning the Chinese LUAD cohort. The corresponding author would provide other relevant data upon reasonable request.

Ethics statement

The animal experimentation conducted in this study received ethics approval from the Ethics Committee of the National Cancer Center/Cancer Hospital, Chinese Academy of Medical Sciences (Approval number: NCC2023A401). Additionally, the experimentation on human tissue samples included in this study was approved by the same Ethics Committee (Approval number: NCC2019C-007).

CRediT authorship contribution statement

Yufeng Guo: Writing – review & editing, Writing – original draft, Visualization, Validation, Software, Methodology, Investigation, Data curation. **Yang Wang:** Methodology, Formal analysis, Data curation. **Jianchun Duan:** Supervision, Resources, Funding acquisition, Data curation, Conceptualization. **Rui Wan:** Software, Methodology, Conceptualization. **Geyun Chang:** Validation. **Xue Zhang:** Data curation. **Zixiao Ma:** Validation. **Hua Bai:** Writing – review & editing, Supervision, Conceptualization. **Jie Wang:** Writing – review & editing, Supervision, Funding acquisition, Data curation, Conceptualization.

Declaration of competing interest

The authors declare that they have no known competing financial interests or personal relationships that could have appeared to influence the work reported in this paper.

Acknowledgments

We thank Dr. Jianming Zeng (University of Macau) and all the members of his bioinformatics team and biotrainee for generously sharing their experience and codes.

Appendix A. Supplementary data

Supplementary data to this article can be found online at https://doi.org/10.1016/j.heliyon.2024.e35940.

References

[1] R.L. Siegel, et al., Cancer statistics, 2021, Ca - Cancer J. Clin. 71 (1) (2021) 7–33.
[2] T.S.K. Mok, et al., Pembrolizumab versus chemotherapy for previously untreated, PD-L1-expressing, locally advanced or metastatic non-small-cell lung cancer (KEYNOTE-042): a randomised, open-label, controlled, phase 3 trial, Lancet 393 (10183) (2019) 1819–1830.
[3] S. Bagchi, R. Yuan, E.G. Engleman, Immune checkpoint inhibitors for the treatment of cancer: clinical impact and mechanisms of response and resistance, Annu. Rev. Pathol. 16 (2021) 223–249.
[4] R. Di Micco, et al., Cellular senescence in ageing: from mechanisms to therapeutic opportunities, Nat. Rev. Mol. Cell Biol. 22 (2) (2021) 75–95.
[5] H.L. Ou, et al., Cellular senescence in cancer: from mechanisms to detection, Mol. Oncol. 15 (10) (2021) 2634–2671.
[6] D.G.A. Burton, A. Stolzing, Cellular senescence: immunosurveillance and future immunotherapy, Ageing Res. Rev. 43 (2018) 17–25.
[7] D. Wang, R.N. DuBois, Immunosuppression associated with chronic inflammation in the tumor microenvironment, Carcinogenesis 36 (10) (2015) 1085–1093.
[8] M. De Cecco, et al., L1 drives IFN in senescent cells and promotes age-associated inflammation, Nature 566 (7742) (2019) 73–78.
[9] M. Simon, et al., LINE1 derepression in aged wild-type and SIRT6-deficient mice drives inflammation, Cell Metabol. 29 (4) (2019) 871–885 e5.
[10] J. Gungabeesoon, et al., A neutrophil response linked to tumor control in immunotherapy, Cell 186 (7) (2023) 1448–1464 e20.
[11] V. Thorsson, et al., The immune landscape of cancer, Immunity 48 (4) (2018) 812–830 e14.
[12] C. Cui, et al., Ratio of the interferon-gamma signature to the immunosuppression signature predicts anti-PD-1 therapy response in melanoma, NPJ Genom Med 6 (1) (2021) 7.
[13] N. Auslander, et al., Robust prediction of response to immune checkpoint blockade therapy in metastatic melanoma, Nat. Med. 24 (10) (2018) 1545–1549.
[14] C.X. Dominguez, et al., Single-cell RNA sequencing reveals stromal evolution into LRRC15(+) myofibroblasts as a determinant of patient response to cancer immunotherapy, Cancer Discov. 10 (2) (2020) 232–253.
[15] S.A. Shukla, et al., Cancer-germline antigen expression discriminates clinical outcome to CTLA-4 blockade, Cell 173 (3) (2018) 624–633 e8.
[16] W. Hugo, et al., Genomic and transcriptomic features of response to anti-PD-1 therapy in metastatic melanoma, Cell 165 (1) (2016) 35–44.
[17] L. Jerby-Arnon, et al., A cancer cell program promotes T cell exclusion and resistance to checkpoint blockade, Cell 175 (4) (2018) 984–997 e24.
[18] W. Zhang, et al., Thiostrepton induces ferroptosis in pancreatic cancer cells through STAT3/GPX4 signalling, Cell Death Dis. 13 (7) (2022) 630.
[19] R. Huang, et al., Dual role of reactive oxygen species and their application in cancer therapy, J. Cancer 12 (18) (2021) 5543–5561.
[20] M. Storer, et al., Senescence is a developmental mechanism that contributes to embryonic growth and patterning, Cell 155 (5) (2013) 1119–1130.
[21] D. Munoz-Espin, et al., Programmed cell senescence during mammalian embryonic development, Cell 155 (5) (2013) 1104–1118.
[22] V. Krizhanovsky, et al., Senescence of activated stellate cells limits liver fibrosis, Cell 134 (4) (2008) 657–667.
[23] M. Ruscetti, et al., NK cell-mediated cytotoxicity contributes to tumor control by a cytostatic drug combination, Science 362 (6421) (2018) 1416–1422.
[24] T.W. Kang, et al., Senescence surveillance of pre-malignant hepatocytes limits liver cancer development, Nature 479 (7374) (2011) 547–551.
[25] K. Rakhra, et al., CD4(+) T cells contribute to the remodeling of the microenvironment required for sustained tumor regression upon oncogene inactivation, Cancer Cell 18 (5) (2010) 485–498.
[26] H. Braumuller, et al., T-helper-1-cell cytokines drive cancer into senescence, Nature 494 (7437) (2013) 361–365.
[27] T. Eggert, et al., Distinct functions of senescence-associated immune responses in liver tumor surveillance and tumor progression, Cancer Cell 30 (4) (2016) 533–547.
[28] D. Di Mitri, et al., Tumour-infiltrating Gr-1+ myeloid cells antagonize senescence in cancer, Nature 515 (7525) (2014) 134–137.
[29] A. Toso, et al., Enhancing chemotherapy efficacy in Pten-deficient prostate tumors by activating the senescence-associated antitumor immunity, Cell Rep. 9 (1) (2014) 75–89.
[30] S. Xiong, L. Dong, L. Cheng, Neutrophils in cancer carcinogenesis and metastasis, J. Hematol. Oncol. 14 (1) (2021) 173.
[31] X. Yu, et al., Neutrophils in cancer: dual roles through intercellular interactions, Oncogene 43 (16) (2024) 1163–1177.
[32] M.A. Giese, L.E. Hind, A. Huttenlocher, Neutrophil plasticity in the tumor microenvironment, Blood 133 (20) (2019) 2159–2167.
[33] M. Gershkovitz, et al., TRPM2 mediates neutrophil killing of disseminated tumor cells, Cancer Res. 78 (10) (2018) 2680–2690.
[34] Z. Granot, et al., Tumor entrained neutrophils inhibit seeding in the premetastatic lung, Cancer Cell 20 (3) (2011) 300–314.
[35] V. De Pinto, et al., Role of cysteines in mammalian VDAC isoforms' function, Biochim. Biophys. Acta 1857 (8) (2016) 1219–1227.
[36] M. Rydzanicz, et al., Novel calcineurin A (PPP3CA) variant associated with epilepsy, constitutive enzyme activation and downregulation of protein expression, Eur. J. Hum. Genet. 27 (1) (2019) 61–69.
[37] S. Fabris, et al., Characterization of oncogene dysregulation in multiple myeloma by combined FISH and DNA microarray analyses, Genes Chromosomes Cancer 42 (2) (2005) 117–127.
[38] A. Escos, et al., p38gamma and p38delta modulate innate immune response by regulating MEF2D activation, Elife 12 (2023).
[39] A. Cuenda, J.J. Sanz-Ezquerro, p38gamma and p38delta: from spectators to key physiological players, Trends Biochem. Sci. 42 (6) (2017) 431–442.
[40] D. Alsina-Beauchamp, et al., Myeloid cell deficiency of p38gamma/p38delta protects against candidiasis and regulates antifungal immunity, EMBO Mol. Med. 10 (5) (2018).
[41] N. Tzenaki, E.A. Papakonstanti, p110delta PI3 kinase pathway: emerging roles in cancer, Front. Oncol. 3 (2013) 40.
[42] N. Tzenaki, et al., High levels of p110delta PI3K expression in solid tumor cells suppress PTEN activity, generating cellular sensitivity to p110delta inhibitors through PTEN activation, Faseb. J. 26 (6) (2012) 2498–2508.
[43] L. Xenou, E.A. Papakonstanti, p110delta PI3K as a therapeutic target of solid tumours, Clin. Sci. (Lond.) 134 (12) (2020) 1377–1397.
[44] S. Ha, B.D. Wang, Molecular insight into drug resistance mechanism conferred by aberrant PIK3CD splice variant in african American prostate cancer, Cancers 15 (4) (2023).
[45] M.J. Fernandez-Sarabia, J.R. Bischoff, Bcl-2 associates with the ras-related protein R-ras p23, Nature 366 (6452) (1993) 274–275.
[46] H.G. Wang, et al., R-Ras promotes apoptosis caused by growth factor deprivation via a Bcl-2 suppressible mechanism, J. Cell Biol. 129 (4) (1995) 1103–1114.
[47] P.E. Hughes, et al., R-Ras regulation of integrin function, Methods Enzymol. 333 (2001) 163–171.
[48] T. Kinashi, et al., Distinct mechanisms of alpha 5beta 1 integrin activation by Ha-Ras and R-Ras, J. Biol. Chem. 275 (29) (2000) 22590–22596.
[49] Y.J. Xu, et al., Inhibition of USP10 induces myeloma cell apoptosis by promoting cyclin D3 degradation, Acta Pharmacol. Sin. 44 (9) (2023) 1920–1931.
[50] L. Agnelli, et al., Molecular classification of multiple myeloma: a distinct transcriptional profile characterizes patients expressing CCND1 and negative for 14q32 translocations, J. Clin. Oncol. 23 (29) (2005) 7296–7306.
[51] W.M. Kuehl, P.L. Bergsagel, Early genetic events provide the basis for a clinical classification of multiple myeloma, Hematology Am Soc Hematol Educ Program (2005) 346–352.
[52] P.L. Bergsagel, et al., Cyclin D dysregulation: an early and unifying pathogenic event in multiple myeloma, Blood 106 (1) (2005) 296–303.
[53] H.Q. Dinh, et al., Coexpression of CD71 and CD117 identifies an early unipotent neutrophil progenitor population in human bone marrow, Immunity 53 (2) (2020) 319–334 e6.
[54] M.E. Shaul, et al., Circulating neutrophil subsets in advanced lung cancer patients exhibit unique immune signature and relate to prognosis, Faseb. J. 34 (3) (2020) 4204–4218.
[55] P.J. Heagerty, Y. Zheng, Survival model predictive accuracy and ROC curves, Biometrics 61 (1) (2005) 92–105.